J Mater Sci (2011) 46:839–845
DOI 10.1007/s10853-010-4826-4

A green method for synthesis of silver nanodendrites

Lei Sun · Aixin Liu · Xiaojun Tao · Yanbao Zhao

Received: 1 April 2010 / Accepted: 10 August 2010 / Published online: 20 August 2010

Abstract A simple, green method was developed for the synthesis of silver nanodendrites by an aqueous chemical route. This method involves the reduction of silver nitrate with absolute alcohol using polyvinyl pyrrolidone (PVP) as the surfactant. UV–vis absorption spectra, X-ray diffraction patterns (XRD) and energy dispersive spectrometry (EDS) suggest the formation of Ag nanoparticles. Transmission electron microscopy (TEM) images show the shape and sizes of the nanoparticles. During the synthesis, it was found that the morphology and size distribution of the as-prepared silver nanoparticles varied with the concentration of the precursor metal salts, reaction time and surfactant ratios. The formation mechanism of Ag nanodendrites was determined based on the investigation of the above reaction parameters. Simple methods, nontoxic chemicals and environmentally benign solvents make this synthesis ideally suited for industrial production.

Keywords Green method · Silver · Nanodendrites · Chemical reduction

Introduction

The preparation of metal nanoparticles is a major research area in nanoscale science and engineering due to their unique chemical and physical properties, such as high catalytic activity, novel electronic, optical and magnetic properties, and their potential applications in biotechnology [1–6]. The architectural control of nanocrystals with specific dimensions and well-defined shapes is important and highly demanded due to the significance of size and shape in determining the intrinsic properties of nanoscale materials. The synthesis of dendritic nanostructures is not as well reported as for other metal nanoparticle morphologies, such as spheres, rods and nanowires [7–13]. Silver nanodendrites are interesting because of their large surface area, which provides good connectivity and makes them useful in diverse applications such as biosensors, chemical sensors, plasmonics and superhydrophobic films [14, 15]. Qiu et al. demonstrated the fabrication of Ag dendrites via an aqueous chemical route based on the spontaneous galvanic displacement between Ag ions and metal solids under hydrothermal conditions [16]. There are also other methods, which have been exploited for the fabrication of noble metal dendrites; these include electrochemical deposition, irradiation reduction, pulse sono-electrochemical techniques, ultrasonic-assisted solution reduction and displacement reactions [17–24]. However, most synthetic methods reported to date rely heavily on organic solvents such as *N*,*N*-dimethylformamide and toxic reducing agents like sodium borohydride, which inevitably results in serious environmental issues for industrial production. To minimize or eliminate pollution to the environment, green methods, which are carried out according to the 12 fundamental principles of green chemistry [25], are required for preparing metal nanoparticles. Utilization of nontoxic chemicals, environmentally benign solvents and renewable materials are some of the key issues that merit important consideration in a green synthetic strategy. The concept of green nanoparticle preparation was first developed by Peng et al. [26], whose report provides a starting point for establishing a precursor/solvent/ligand database for designing optimized green-chemical synthetic approaches

L. Sun (✉) · A. Liu · X. Tao · Y. Zhao
Key Laboratory for Special Functional Materials of Ministry of Education, Henan University, Kaifeng 475004, People's Republic of China
e-mail: sunlei@henu.edu.cn

for high-quality nanocrystals. A green method for the preparation of nanoparticles should be evaluated from three aspects: the solvent, the reducing agent and the stabilizing agent. In this paper, we present a simple and green method for the preparation of silver nanodendrites using absolute alcohol as the reducing agent and polyvinyl pyrrolidone (PVP) as the stabilizing agent, both of which are nontoxic chemicals. The reaction is carried out in an aqueous solution in a process that is benign to the environment. We also investigated the effects of the concentration of the precursor metal salts, reaction time and surfactant ratios on the morphology and size distribution of the as-prepared silver nanoparticles.

Experimental

Chemicals and instruments

Analytical grade silver nitrate ($AgNO_3$), absolute alcohol and PVP (MW 40,000) were used as starting materials, without further purification. $AgNO_3$ was purchased from Chemical Reagent Corporation of Chinese National Medical Group. Absolute alcohol was purchased from Ante Chemical Reagent Corporation (Anhui, China). PVP was purchased from Lanji Corporation (Shanghai, China). Distilled water was used throughout the experiment. A Unicarn 540 UV–visible spectrophotometer was used to conduct optical measurements. The analysis was performed in silica cuvettes (1 cm path length), using distilled water as a reference solvent. Transmission electron microscopy (TEM) images were obtained using a JEOL JEM-100CX transmission electron microscope. The samples were prepared by placing a drop of primary sample on a copper grid. The TEM samples were allowed to dry completely at ambient temperature. X-ray diffraction (XRD) patterns were collected on a Philips X'pert Pro X-ray powder diffractometer using Cu Kα radiation ($\lambda = 1.5418$ Å). The operation voltage and current were 40 kV and 40 mA, respectively. Energy dispersive spectra (EDS) were recorded with an OXFORD Link ISIS X-ray energy dispersive spectrometer.

Synthesis of silver nanodendrites

In a typical procedure, 0.1359 g of PVP and 0.4077 g of $AgNO_3$ were separately dissolved in 20 and 15 mL of distilled water, respectively. Both solutions were mixed in a 100 mL round-bottomed flask to form a homogeneous mixture using electromagnetic stirring. Then, 5 mL of absolute alcohol was added to the above solution. Afterward, the chemical reduction process was performed by heating the sample for 2 h at 70°C, causing the solution to become wine colored due to the formation of silver nanoparticles. The concentration of $AgNO_3$ in the solution in this procedure was 1%. For morphological and structural investigations, other solution concentrations were also obtained.

Results and discussion

Effect of reactant concentrations

During the preparation of silver nanoparticles, the concentration of $AgNO_3$ plays an important role. It has a great effect on the morphology and size of the silver nanoparticles. Three samples were prepared with different $AgNO_3$ concentrations of 0.3, 1 and 10%, respectively. The $AgNO_3$/PVP mass ratio was the same for all of the above procedures, and was 1/3. The reaction time for all of these experiments was 2 h. The formation of Ag can be confirmed from the study of the UV–vis spectra of the products using different concentrations of $AgNO_3$ as shown in Fig. 1(a, 0.3%; b, 1%; c, 10%) with strong absorbance peaks in the visible range indicative of Ag nanoparticles. Figure 1d contains the UV–vis spectrum of the original mixed solution of PVP and $AgNO_3$, which does not show any absorption in the range of 800–300 nm, confirming that no nanoparticles were initially present. Silver metal nanoparticles are known to have intense surface plasmon absorption bands in the visible region [27]. The shape of these plasmon bands are symmetrical, suggesting that the nanoparticles are well dispersed and spherical since the aggregation of nanoparticles leads to red-shifted and broadened plasmon absorptions [28]. The absorption spectrum of the silver nanoparticles synthesized at a low

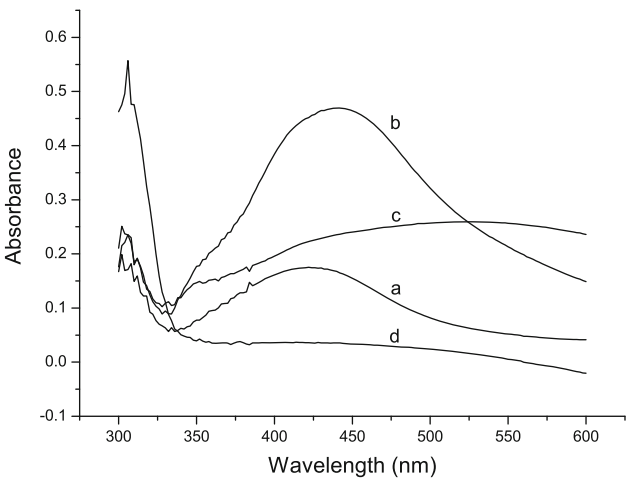

Fig. 1 UV-vis spectra of silver nanoparticles at $AgNO_3$ concentrations of (*a*) 0.3%, (*b*) 1%, (*c*) 10%, and (*d*) the mixed solution of PVP and $AgNO_3$ before reduction

concentration of $AgNO_3$ (0.3%) shows a broad band around 423 nm (Fig. 1a). When the concentration is 1 and 10%, the corresponding absorption plasmon bands are 438 nm and 520–570 nm, respectively. The increase in concentration of the initial complex in the range of 0.3–10% leads to a red shift of the absorption plasmon band from 423 to 520–570 nm, suggesting that the size of the particles increases and the shape changes. The absorption band of Fig. 1c is significantly broader due to the presence of synthesized silver nanodendrites, which are shown in Fig. 2c.

From the TEM images of the Ag nanopartices (Fig. 2), it can be seen that the shape and size of the particles vary greatly with $AgNO_3$ concentration. Isotropic silver nanoparticles with sizes ranging from 20 to 30 nm (Fig. 2a) can be observed at low concentrations of $AgNO_3$. When the concentration of $AgNO_3$ is increased to 1%, hexagonal and triangular particles appear, evidencing an evolution of shape (Fig. 2b), while the size of the nanoparticles increases to 80–100 nm. At a high concentration of 10% $AgNO_3$, dendritic nanostructures are observed (Fig. 2c). The selected area electron diffraction (SAED) patterns shown in the insets of Fig. 2a and b exhibit Debye–Scherrer rings, which could be indexed to the (111), (200) and (220) planes of the face-centered cubic (fcc) crystalline lattice of Ag. The indexed SAED results for the fcc phase of the Ag dendritic nanostructures is shown in the inset of Fig. 2c.

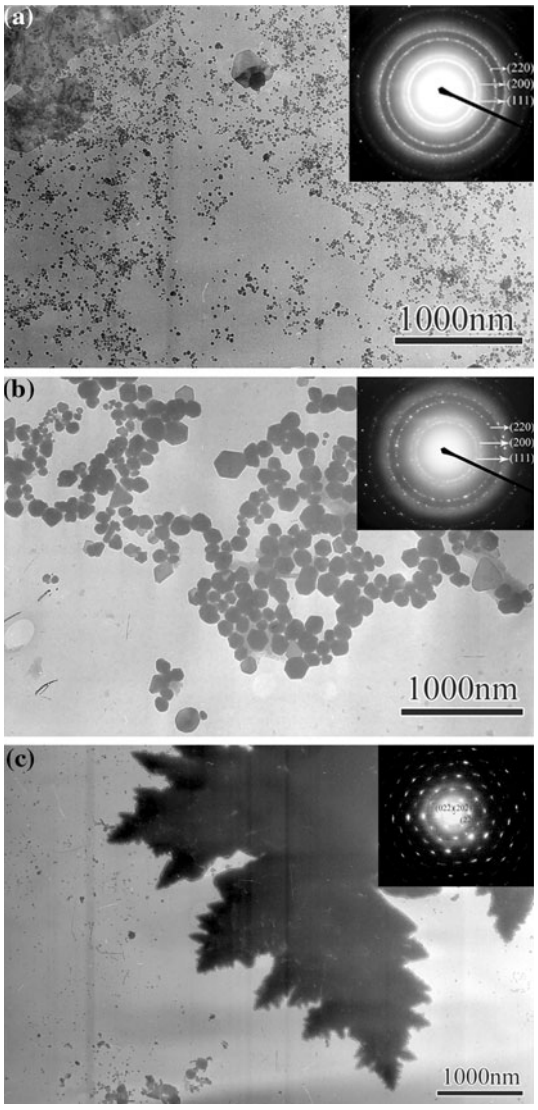

Fig. 2 TEM images and *inset* SAED patterns of silver nanoparticles synthesized at different concentrations of $AgNO_3$, with **a** 0.3%, **b** 1% and **c** 10%

Figure 3 shows the XRD patterns of Ag nanoparticles synthesized at different $AgNO_3$ concentrations of (a) 0.3%, (b) 1% and (c) 10%. It can be seen that the peaks at $2\theta = 38.2°$, 44.2°, 64.6°, 77.4° and 81.6° are assigned to diffraction from the (111), (200), (220), (311) and (222) lattice planes of silver, respectively, which is indicative of cubic silver (Joint Committee on Powder Diffraction Standards File no. 87-0720). Thus, it is concluded that Ag nanocrystals were successfully prepared in these reactions. The crystalline size of the Ag nanoparticles corresponding to the XRD patterns of a, b and c was 7.2, 15.7 and 23.4 nm, respectively, and was calculated from the half width of the diffraction peaks using the Scherrer formula. This result does not reconcile with the average size estimated from TEM images (Fig. 2). This is due to the fact that XRD gives the crystallite size, while TEM shows the apparent particle size. In some cases, one nanoparticle observed in TEM may contain several nanocrystals. The peak at $2\theta = 21.2°$ can be assigned to the amorphous diffraction from the organic coating layer of PVP. It also can be seen from Fig. 3 that the diffraction pattern broadens and the intensity becomes weaker with

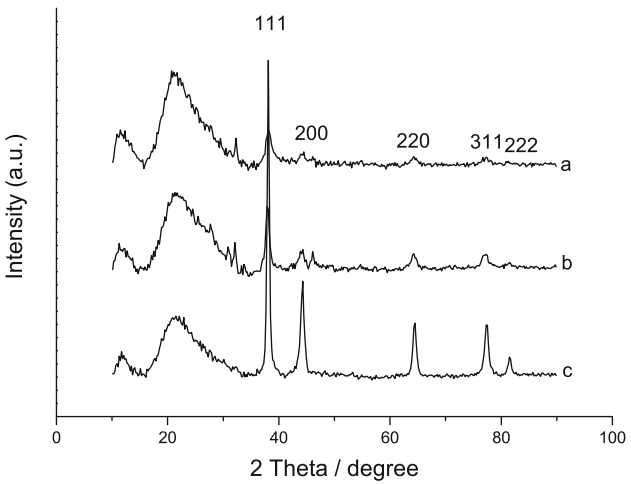

Fig. 3 XRD patterns of silver nanoparticles synthesized at different concentrations of $AgNO_3$, with (*a*) 0.3%, (*b*) 1% and (*c*) 10%

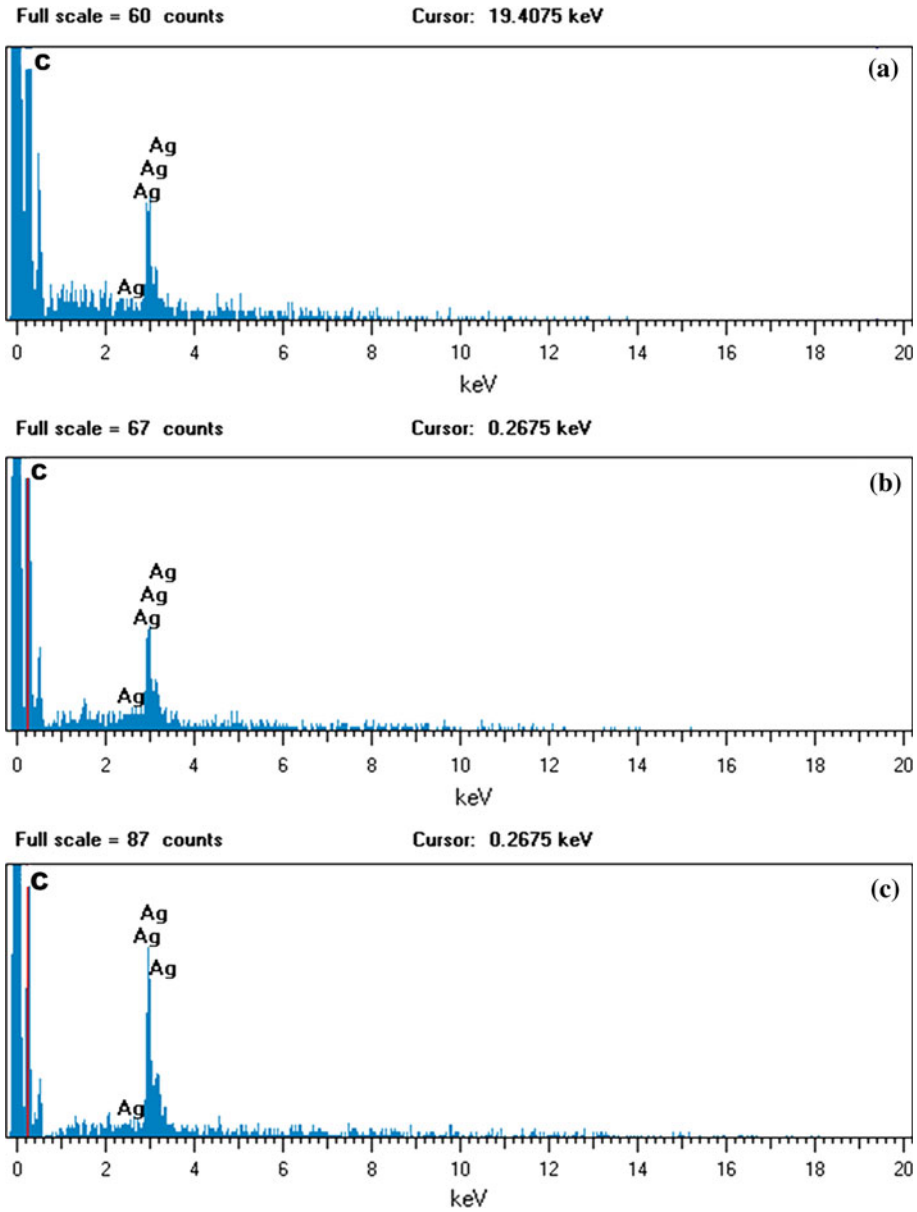

Fig. 4 EDS spectra of silver nanoparticles synthesized at different concentrations of $AgNO_3$, with **a** 0.3%, **b** 1% and **c** 10%

decreasing $AgNO_3$ concentration, which suggests that the Ag nanoparticles become smaller. This trend is consistent with the TEM observation.

Figure 4 shows EDS spectra of nanoparticles synthesized with different $AgNO_3$ concentrations of (a) 0.3%, (b) 1% and (c) 10%. The presence of Ag can clearly be seen, indicating that the as-prepared powders are composed of Ag nanoparticles. Figure 4 also shows the presence of C, which is derived from the conductive adhesive base.

Effect of surfactant ratio

The effect of PVP on the morphologies of the Ag nanoparticles was also investigated. The experiment was processed at a $AgNO_3$ concentration of 0.3% with no PVP present in the reaction. When the color of the solution finally became orange-red, the reaction had lasted for 6 h. This indicates that when the surfactant PVP is absent, the reduction process is very slow. PVP is a water-soluble polymer containing many amino groups, which may bond with metallic ions. This leads to the formation of a unique PVP-Ag^+ complex precursor system in the solution. The use of precursor amine complexes of silver, instead of merely Ag^+ ions, provides a flexible strategy to control the reduction of silver ions. The reduction potential for an Ag^+/Ag (aqueous) system is +0.7996 V, but the reduction potential for the redox pair of $Ag(NH_3)^+/Ag$(aqueous) is +0.373 V [29]. This makes the reduction of Ag^+ amine complex possible with mild reducing agents such as absolute alcohol. Thus, the reaction progress is slower in

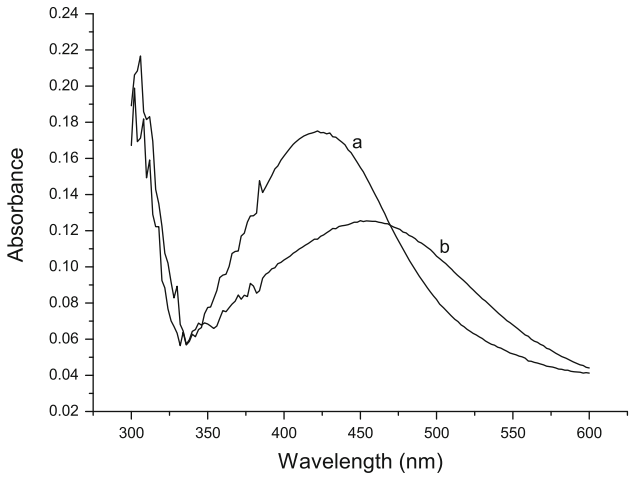

Fig. 5 UV–vis spectra of silver nanoparticles: (*a*) with PVP, (*b*) in the absence of PVP

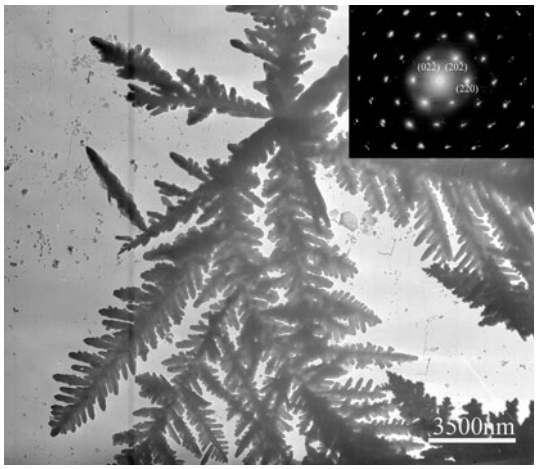

Fig. 6 TEM images and *inset* SAED patterns of silver dendritic nanostructures synthesized in the absence of PVP

the absence of PVP. The UV–vis spectra of this experiment are shown at Fig. 5. A red shift of the absorption plasmon band appears in the absence of PVP, suggesting that the size of particles is increased. It can be concluded that the reduction rate has an effect on the particles size; larger particles are generated when the reduction process is very slow. Ag dendritic nanostructures are observed in TEM images (Fig. 6). The average length and breadth of the Ag dendritic branches are about 900 and 350 nm, respectively. From SAED patterns inserted in Fig. 2a, it can be seen that when the shape of the particles is spherical, they are polycrystalline. However, when the particles have a dendritic morphology, they exhibit a single crystalline structure (Fig. 6). SAED patterns inset in Fig. 6 also indicate that Ag dendritic nanostructures exhibit an fcc crystalline phase.

Effect of reaction time

Due to the significant effect of the reaction time on the shape and size of the product, an experiment using various reaction times was carried out with a $AgNO_3$ concentration of 1% and a $AgNO_3$/PVP mass ratio of 1/3. The experiment was processed for a total of 12 h and samples were extracted at different times for UV–vis absorption measurements and TEM observation. Figure 7 shows the UV–vis spectra and TEM images of Ag nanoparticles prepared with different reaction times. From Fig. 7 a, it is apparent that many nanoparticles exist in the solution and the branches of the Ag dendritic nanostructures are small and fine when the reaction time is only 1 h. As shown in Fig. 7 b–e, with the extension of reaction time, the size of the nanoparticles becomes larger and the branches of the Ag dendritic nanostructures become coarser and longer. The phenomena of red-shifted and broadened plasmon absorptions of the Ag nanoparticles were observed in conjunction with the morphology change evident from the TEM. It also can be seen from Fig. 7 that the intensity of the UV–vis spectra becomes weak as the Ag nanoparticle concentration decreases.

Formation mechanism analysis

Absolute alcohol is a very weak reducing agent, which is expected to favor the formation of dendritic nanostructures. Figure 8 is a schematic illustration of the formation of silver nanodendrites. When the concentration of $AgNO_3$ was increased, $AgNO_3$ was reduced to form more silver isotropic particles that came into contact with one another more easily to form larger objects such as dendrites. PVP can prevent the aggregation of Ag nanoparticles. At low $AgNO_3$ concentrations (0.3%), only Ag nanoparticles were formed in the presence of PVP. However, when PVP was absent, there was no surfactant to prevent the diffusion of newly formed particles onto the surface of existing particles, thereby allowing the formation of tree-like structures. At high $AgNO_3$ concentrations (1, 10%), there was insufficient PVP to prevent the assembly of Ag nanoparticles, which subsequently developed into dendritic nanostructures.

Conclusions

In summary, silver dendrites were prepared by the reduction of $AgNO_3$ with absolute alcohol using PVP as the surfactant with a simple, green method. It was found that reaction time, PVP and the $AgNO_3$ concentration played important roles in controlling the growth morphology of the silver particles. The UV–vis spectra, XRD patterns, EDS and TEM images of as-prepared samples at various

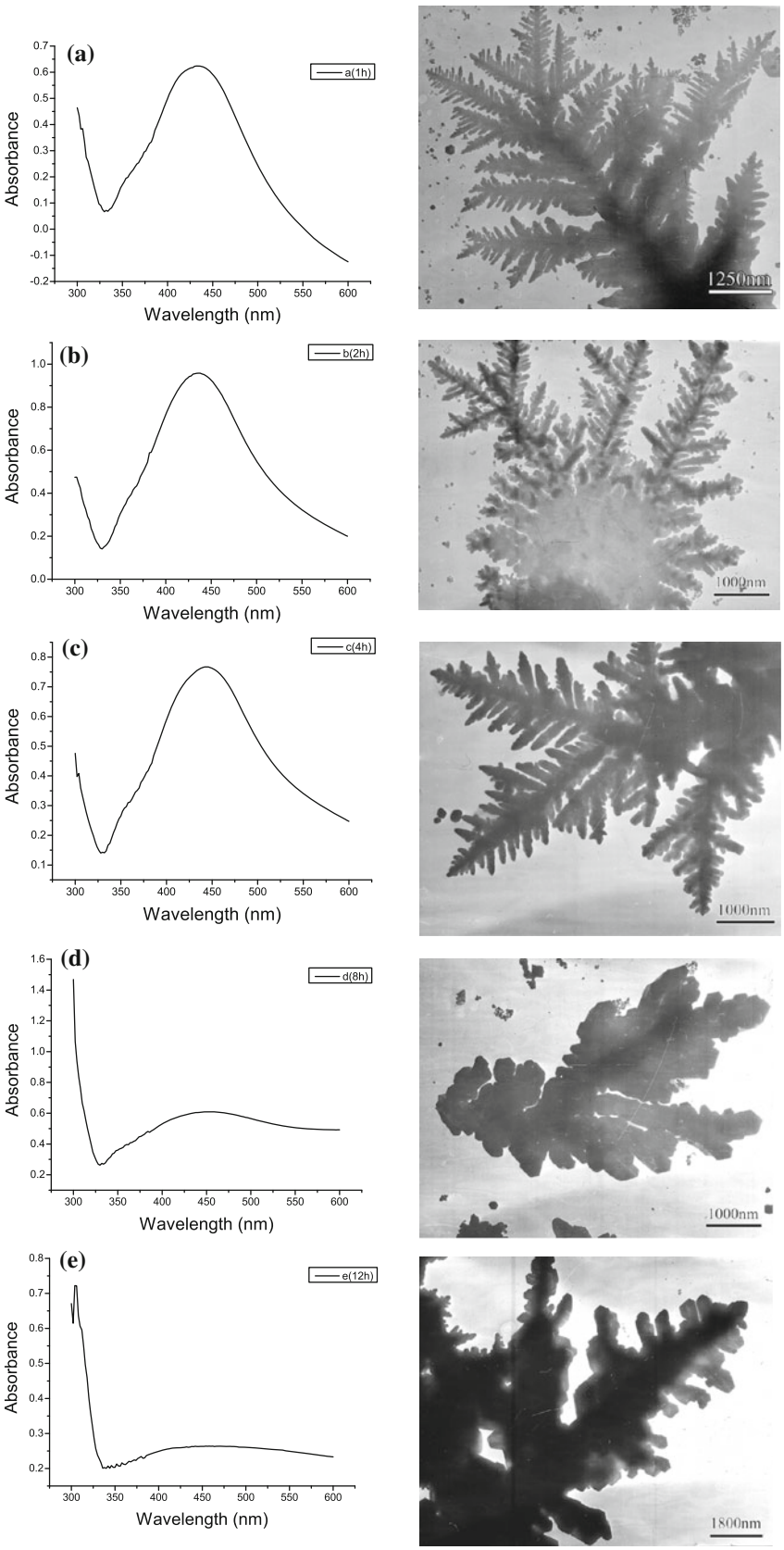

Fig. 7 UV–vis spectra and TEM images of Ag dendritic nanostructures prepared with different reaction times: **a** 1 h, **b** 2 h, **c** 4 h, **d** 8 h, and **e** 12 h

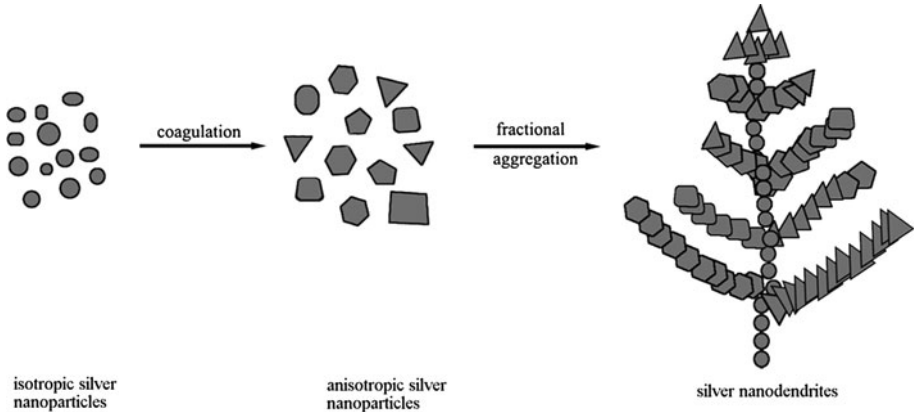

Fig. 8 Schematic illustration of the formation mechanism of Ag nanodendrites

concentrations confirm the existence of Ag particles with varying morphologies. When the particle morphology is spherical, they are polycrystalline, and when the particles have a dendritic nanostructure, they exhibit single crystallinity.

Acknowledgments The authors are grateful for the financial support provided by the National Science Foundation of China (50701016) and the Foundation of Education Department of Henan Province (2007150008, 2008B150003). We are also grateful to James Goebl at University of California, Riverside for the assistance in text revision.

References

1. Volokitin Y, Sinzig J, Jongh LJ, Schmid G, Vargaftik MN, Moiseev II (1996) Nature 384:621
2. Braun E, Eichen Y, Sivan U, Ben-Yoseph G (1998) Nature 391:775
3. Kabashin AV, Meunier M, Kingston C, Luong JHT (2003) J Phys Chem B 107:4527
4. Chimentao RJ, Medina F, Sueiras JE, Fierro JLG, Cesteros Y, Salagre P (2007) J Mater Sci 42:3307. doi:10.1007/s10853-006-0570-1
5. Chen D, Qiao X, Qiu X, Chen J (2009) J Mater Sci 44:1076. doi:10.1007/s10853-008-3204-y
6. Hayward RC, Saville DA, Aksay IA (2000) Nature 404:56
7. Chen C, Wang L, Li R, Jiang G, Yu H, Chen T (2007) J Mater Sci 42:3172. doi:10.1007/s10853-007-1594-x
8. Bera T, Ramachandrarao P (2009) J Mater Sci 44:2264. doi:10.1007/s10853-008-2861-1
9. Pastoriza-Santos I, Liz-Marzan LM (2000) Pure Appl Chem 72:83
10. Yener DO, Sindel J, Randall CA, Adair JH (2002) Langmuir 18:8692
11. Sun Y, Mayers B, Herricks T, Xia Y (2003) Nano Lett 3:955
12. Zhao Y, Jiang Y, Fang Y (2006) Spectochim Acta A 65:1003
13. Tsuji M, Nishizawa Y, Matsumoto K, Kubokawa M, Miyamae N, Tsuji T (2006) Mater Lett 60:834
14. Zhao N, Shi F, Wang ZQ, Zhang X (2005) Langmuir 21:4713
15. Geddes CD, Parfenov A, Gryczynski I, Lakowicz JR (2003) J Phys Chem B 107:9989
16. Wang Z, Zhao Z, Qiu J (2008) J Phys Chem Solids 69:1296
17. Kang ZH, Wang EB, Lian SY, Mao BD, Chen L, Xu L (2005) Mater Lett 59:2289
18. Zhou Q, Wang S, Jia NQ, Liu L, Yang JJ, Jiang ZY (2006) Mater Lett 60:3789
19. Zhou Y, Yu SH, Wang CY, Li XG, Zhu YR, Chen ZY (1999) Adv Mater 11:850
20. Wang SZ, Xin HW (2000) J Phys Chem B 104:5681
21. He R, Qian XF, Yin J, Zhu ZK (2003) Chem Phys Lett 369:454
22. Zhu JJ, Liu SW, Palchik O, Koltypin Y, Gedanken A (2000) Langmuir 16:6396
23. Chairam S, Poolperm C, Somsook E (2009) Carbohydr Polym 75:694
24. Asta M, Beckermann C, Karma A, Kurz W, Napolitano R, Plapp M, Purdy G, Rappaz M, Trivedi R (2009) Acta Mater 57:941
25. Anastas PT, Warner JC (1998) Green chemistry: theory and practice. Oxford University Press, New York
26. Qu L, Peng ZA, Peng X (2001) Nano Lett 1:333
27. Henglein A, Giersig M (1999) J Phys Chem B 103:9533
28. Lin SY, Liu SW, Lin CM, Chen CH (2002) Anal Chem 74:330
29. Manoth M, Manzoor K, Patra MK, Pandey P, Vadera SR, Kumar N (2009) Mater Res Bull 44:714